LETTERS
PUBLISHED ONLINE: 17 MARCH 2013 | DOI: 10.1038/NMAT3596
nature materials

Surface chemistry mediates thermal transport in three-dimensional nanocrystal arrays

Wee-Liat Ong[1†], Sara M. Rupich[2†], Dmitri V. Talapin[2*], Alan J. H. McGaughey[1,3] and Jonathan A. Malen[1,3*]

Arrays of ligand-stabilized colloidal nanocrystals with size-tunable electronic structure are promising alternatives to single-crystal semiconductors in electronic, optoelectronic and energy-related applications[1–5]. Hard/soft interfaces in these nanocrystal arrays (NCAs) create a complex and uncharted vibrational landscape for thermal energy transport that will influence their technological feasibility. Here, we present thermal conductivity measurements of NCAs (CdSe, PbS, PbSe, PbTe, Fe_3O_4 and Au) and reveal that energy transport is mediated by the density and chemistry of the organic/inorganic interfaces, and the volume fractions of nanocrystal cores and surface ligands. NCA thermal conductivities are controllable within the range 0.1–0.3 $W\,m^{-1}\,K^{-1}$, and only weakly depend on the thermal conductivity of the inorganic core material. This range is 1,000 times lower than the thermal conductivity of silicon, presenting challenges for heat dissipation in NCA-based electronics and photonics. It is, however, 10 times smaller than that of Bi_2Te_3, which is advantageous for NCA-based thermoelectric materials.

Colloidal nanocrystals self-assemble into NCAs with electronic and optical properties that can be broadly tuned by nanocrystal composition and size[1–4,6–8]. To be considered as viable replacements for traditional semiconductors, NCA-based technologies must also meet thermal management demands as high operating temperatures degrade device performance and lifetime. Thermal conductivity (k) quantifies a material's ability to dissipate heat and relates temperature gradient (∇T) to heat flux ($\mathbf{q}$) through Fourier's law, $\mathbf{q} = -k\nabla T$. In metals, most heat is carried by electrons, whereas in semiconductor and insulating crystals, thermal conductivity arises from the transport and scattering of quantized vibrations that are born from the periodic atomic lattice, that is, phonons. Our NCAs are non-metallic and have a vibrational structure that is complicated by compositional heterogeneity and periodicity at two length scales: the atomic lattice within each core and the array of periodic cores separated by ligand monolayers. Studies of planar self-assembled monolayer (SAM) junctions show that surface chemistry can control energy transport at the interface between two solids[9], but does it also influence the thermal conductivity of a bulk three-dimensional solid with a complex network of internal interfaces? We herein report on the hitherto unknown thermal transport properties of NCAs, using systematic thermal conductivity measurements complemented by heat capacity measurements and atomistic simulations.

A series of NCAs was prepared with varying core diameters, core materials and ligand groups (Table 1) through spin-coating concentrated colloidal solutions onto silicon wafers[6]. During film formation, the monodisperse nanocrystals self-assembled into arrays, as seen in Fig. 1a–c. For thermal conductivity measurements, the NCA films were coated with a gold transducer (150–250 nm thick) by electron-beam evaporation.

The specific heat capacity (C_p) of the NCAs was determined using differential scanning calorimetry (DSC). The measured C_p varies with temperature and nanocrystal size as shown for a diameter series of PbS NCAs in Fig. 1d,e. The abrupt change in slope in C_p around 200 K is the result of a glassy transition of the oleate ligands[10,11], as these unsaturated hydrocarbon tails do not crystallize at the nanocrystal surface. In contrast, the CdSe NCAs capped with long saturated hydrocarbon chains (that is, *n*-tetradecylphosphonic acid) can form ordered domains at the nanocrystal surface, indicated by sharp peaks in the DSC curves in Supplementary Fig. S1. We find that C_p can be estimated from a weighted average based on the constituent mass fractions determined from thermogravimetric analysis (TGA; Supplementary Fig. S2) and the bulk specific heat capacities of the inorganic core material and the ligand (Fig. 1e).

Molecular dynamics simulations and harmonic lattice dynamics calculations were performed to elucidate how the vibrational structure of a nanocrystal is related to its constituent core and ligands (see Supplementary Information). The vibrational density of states (vDOS) of a 2.8-nm-diameter Au nanocrystal and its constituent Au core and dodecanethiol ligands are shown in Fig. 2. The C_p of solids results from occupation of the vDOS according to Bose–Einstein statistics. All core vibrational states overlap with ligand states below the thermal activation frequency at 300 K. Higher-frequency ligand states have no corresponding core states to overlap with at higher temperatures. These two general features will be found for core materials with a similar Debye temperature to Au (165 K). Similarities in the vDOS of the nanocrystal and its components thus explain why the measured C_p is consistent with the estimate based on mass fraction. In this work, experimental thermal conductivity measurements were carried out to understand how this vibrational structure influences thermal transport.

To measure the thermal conductivity of the NCA thin films, we employed the frequency-domain thermal reflectance (FDTR) technique detailed in the Methods[12]. For CdSe NCAs, the measured thermal conductivities are independent of film thickness at temperatures of 10, 77 and 300 K, as shown in Supplementary Fig. S3a (room-temperature measurements for other NCAs are shown in Supplementary Fig. S3b). This result suggests that thermal transport in NCAs is dominated by diffusive phonons with short mean-free paths. Furthermore, the thickness invariance indicates that our measured values are bulk-like and not distorted by thermal resistances at the Au/NCA and NCA/Si boundaries.

[1]Department of Mechanical Engineering, Carnegie Mellon University, Pittsburgh, Pennsylvania 15213, USA, [2]Department of Chemistry, University of Chicago, Chicago, Illinois 60637, USA, [3]Department of Materials Science and Engineering, Carnegie Mellon University, Pittsburgh, Pennsylvania 15213, USA. †These authors contributed equally to this work. *e-mail: dvtalapin@uchicago.edu; jonmalen@andrew.cmu.edu.

Table 1 | Nanocrystals and ligands used for the preparation of NCA thin films.

Core	Diameter (nm)	Ligand	Type of material
CdSe	3.5, 4.1	*n*-tetradecylphosphonic acid	Semiconductor
	5.2	*n*-octylphosphonic acid	
	4.8	$(N_2H_5)_2In_2Se_4$	
PbS	3.5, 4.5, 5.2	Oleic acid	Semiconductor
	7.5	Oleic acid, nonanoic acid, Na_3AsS_3, N_2H_4	
PbSe	7.5	Oleic acid	Semiconductor
PbTe	7.5	Oleic acid	Semiconductor
Fe_3O_4	4.5, 8	Oleic acid	Metal oxide
Au	4.5	*n*-dodecanethiol	Metal

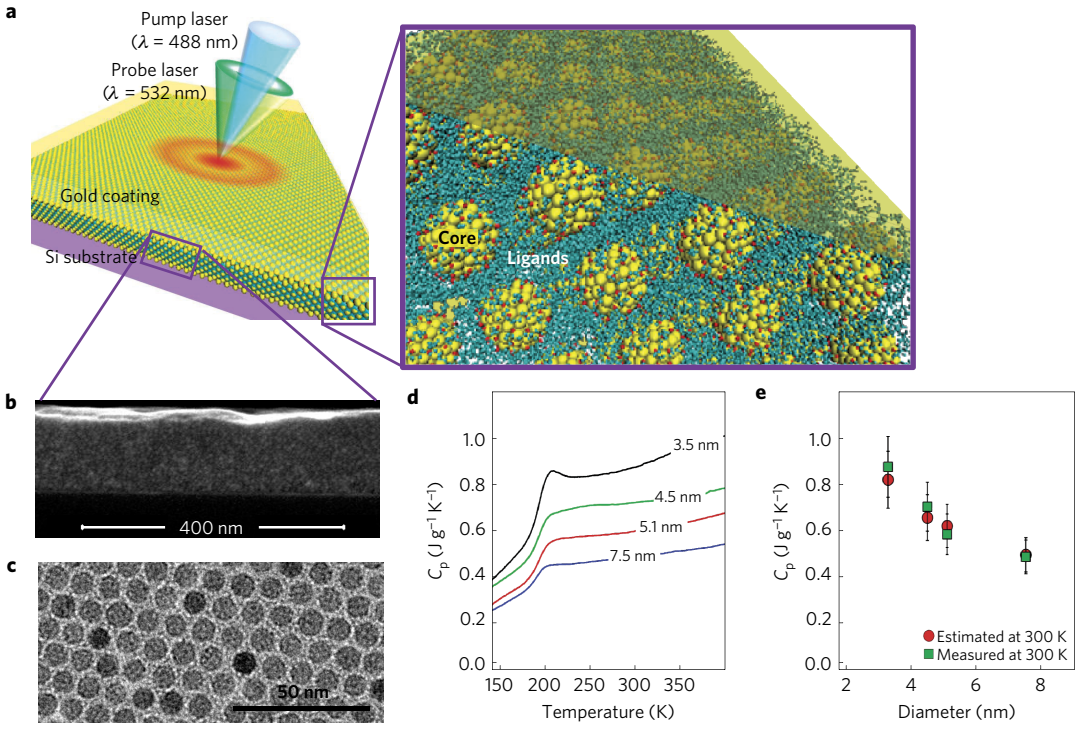

Figure 1 | Structure and heat capacity of NCA films. a, Schematic of a gold-coated NCA film where an intensity-modulated pump laser periodically heats the sample and a probe laser senses the resultant temperature change by thermoreflectance to measure thermal conductivity (see Methods for FDTR details). The magnified view to the right depicts the NCA thin film. **b**, SEM cross-sectional image of a 7.5-nm-diameter PbS NCA film. **c**, Planar TEM image of an 8-nm-diameter Fe_3O_4 NCA film showing a regular close-packed arrangement. **d**, Specific heat capacity data as a function of temperature for a diameter series of PbS nanoparticles coated with oleic acid ligands. **e**, The specific heat capacity of a NCA at 300 K can be estimated as a mass-weighted function of the specific heat capacities of the core material (C_{core}) and the ligand (C_{Ligand}) such that, $C_P = m_{core}C_{core} + m_{Ligand}C_{Ligand}$, where m_{core} is the mass fraction of the core and m_{Ligand} is the mass fraction of the ligand. The plot shows the measured and estimated values using bulk values of PbS ($C_{core} = 0.19\,J\,g^{-1}\,K^{-1}$, ref. 24) and oleic acid ($C_{Ligand} = 2.043\,J\,g^{-1}\,K^{-1}$, ref. 30). Error bars represent uncertainty from DSC and TGA measurements.

The measured thermal conductivity as a function of core diameter for CdSe, PbS, PbSe, Au and Fe_3O_4 NCAs is shown in Fig. 3a. Regardless of the core material, the NCA thermal conductivity increases with increasing diameter. The inset of Fig. 3a shows that k_{NCA} is insensitive to the core-material bulk thermal conductivity for nanocrystals of the same diameter. To understand these trends, effective medium approximations (EMAs) of thermal conductivity are compared with data for PbS NCAs in Fig. 3b (see Supplementary Information for EMA details). EMAs predict thermal conductivity of composites in terms of the constituent volume fractions and thermal conductivities. Specification of the ligand thermal conductivity is challenging because the ligand molecules are covalently bound to the inorganic cores through metal–ligand bonds, thus creating structure in the NCA that is absent in pure ligand molecules. To estimate the thermal conductivity of bound oleate ligands, we used FDTR to independently measure the thermal conductivity of Pb oleate (a waxy solid at 300 K). We find $k_{Pb\ oleate} = 0.13 \pm 0.02\,W\,m^{-1}\text{-}K^{-1}$, which is 40% lower than liquid oleic acid[13]. With this value, effective medium theory[14], a specific EMA that assumes a random distribution of the two phases, captures the increasing trend due to increasing core volume fraction, yet severely overestimates k_{NCA}. The Maxwell Euken[14] (ME) EMA assumes dispersed spheres in a continuous matrix, yet still overestimates k_{NCA} despite more accurately representing the NCA structure.

It is known that thermal interface conductance h between the phases in a composite can reduce its effective thermal conductivity. We fit a version of the ME model, modified by Hasselman and Johnson[15] (HJ–ME) with the addition of a finite h, to predict k_{NCA}. For a best fit h of $140^{+170}_{-80}\,MW\,m^{-2}\,K^{-1}$, HJ–ME agrees well

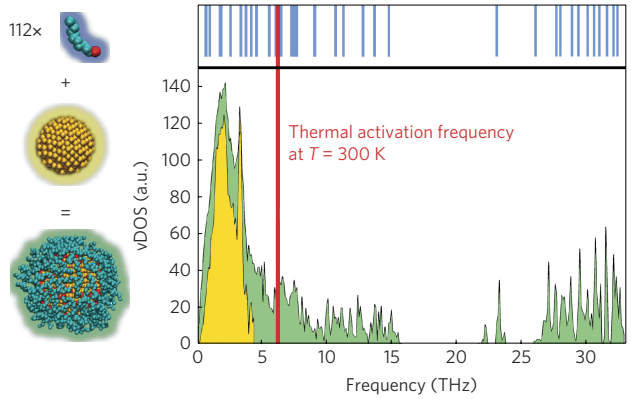

Figure 2 | vDOS of a 2.8-nm-diameter Au nanocrystal and its individual constituents (Au core and a dodecanethiol ligand) predicted from lattice dynamics calculations. The blue vertical lines represent the vibrational spectrum of one ligand. The yellow region is the vDOS of the Au core, which is enclosed in the green vDOS of the nanocrystal. The vertical red line represents the thermal activation frequency ($k_B T/h$) at a temperature of 300 K (k_B is the Boltzmann constant and h is the Planck constant).

with our data, as shown in Fig. 3b. This value is comparable with direct measurements of thermal conductance through a planar alkanethiol-SAM/Au interface (220 ± 100 MW m^{-2} K^{-1})[16]. SAM junctions[9,17] have a lower measured thermal conductance (25–70 MW m^{-2} K^{-1}) because they include additive resistances due to the SAM itself and two interfaces. Amendments to HJ–ME by Minnich *et al.*[18] include reduced phonon mean-free paths due to nanostructuring, yet do not improve the fit because k_{NCA} is insensitive to the core thermal conductivity (Fig. 3a). Hence, the increase of k_{NCA} with nanocrystal diameter can be rationalized on the basis of decreased interface density and increased core volume fraction that accompany increased core diameter.

The EMA analysis points to h as a crucial factor in explaining k_{NCA} and temperature-dependent measurements of k_{NCA} can provide further insight. The thermal conductivities of PbS, PbSe, PbTe and CdSe NCAs increase from 10 to 200 K and plateau above 200 K, as shown in Fig. 3c,d. This behaviour suggests that interfacial vibrational energy transport at the measured temperatures is dominated by elastic events, whereby the frequencies of the interacting states are the same, and can be understood by considering the vDOS. Below a temperature of 200 K, which is near the Debye temperatures (θ_D) of CdSe, PbS, PbSe and PbTe ($\theta_{D,CdSe} = 182$ K, ref. 19; $\theta_{D,PbS} = 225$ K, $\theta_{D,PbSe} = 175$ K, $\theta_{D,PbTe} = 136$ K, ref. 20) increasing the temperature increases the populations of vibrational states with frequencies that are common to the cores and ligands. When the temperature increases beyond the core θ_D, the vibrational frequencies common to the cores and ligands are fully activated. Additional higher-frequency ligand states continue to be activated (Fig. 2), but as these ligand states do not have core states to couple with elastically, the thermal conductivity plateaus. This hypothesis is supported by the thermal conductivity of Fe_3O_4 NCAs, which plateaus above 300 K (Fig. 3c,d), consistent with Fe_3O_4 having a significantly higher Debye temperature ($\theta_{D,Fe3O4} > 350$ K, ref. 21) than PbS, PbSe, PbTe or CdSe. The critical role of the interface in the temperature dependence is confirmed by the thermal conductivity of Pb oleate (oleate is the ligand in the Fe_3O_4, PbS, PbSe and PbTe NCAs), which shows an earlier plateau that cannot be the lone source of the variable NCA plateaus (see temperature dependence of h in the

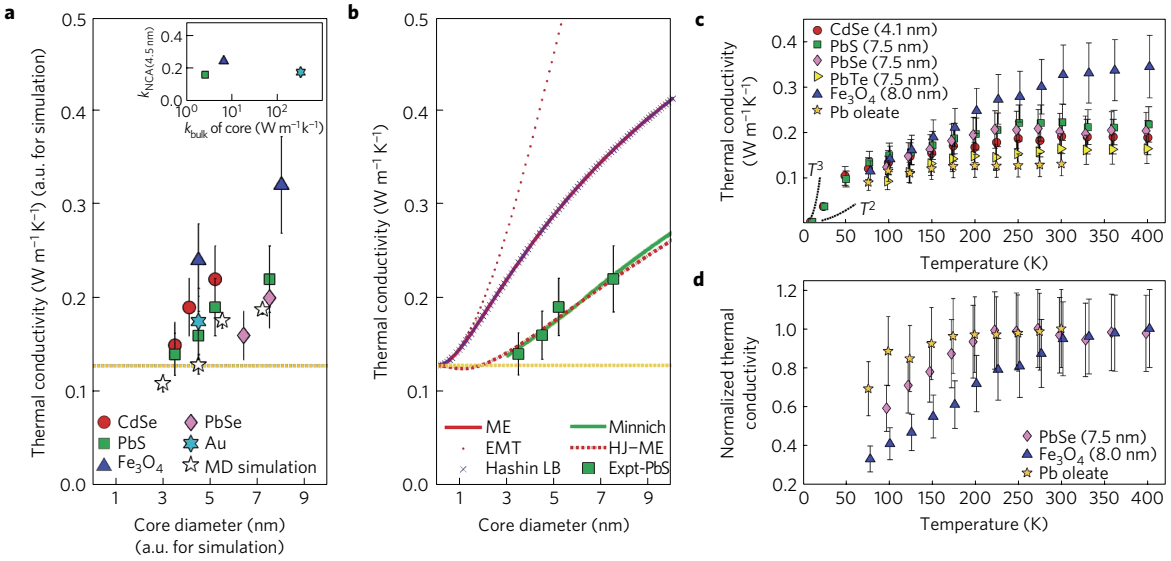

Figure 3 | Effects of NCA geometry and temperature on thermal conductivity. a, Diameter series data for various NCAs have increasing thermal conductivity with core diameter regardless of core composition. The trend of the molecular dynamics (MD) simulation results agrees with the experimental data. The inset shows that k_{NCA} does not strongly depend on the thermal conductivity of the bulk core material. The orange dotted line here and in **b** is the thermal conductivity of Pb oleate at 300 K. **b**, EMAs (effective medium theory[14] (EMT); Hashin LB, ref. 31) cannot explain the PbS NCA data without the use of a finite thermal conductance at the core/ligand interface, which is integral to HJ–ME and Minnich models (see Supplementary Information for details of EMAs). These models clarify that increased k_{NCA} results from decreased interface density (from 4.37×10^8 m^2 m^{-3} to 3.43×10^8 m^2 m^{-3}) and increased core volume fraction (from 0.24 to 0.43) over the diameter range 3.3–7.5 nm. **c**, Temperature series for CdSe (diameter = 4.1 nm, $\theta_{D,CdSe} = 182$ K; ref. 19), PbS (diameter = 7.5 nm, $\theta_{D,PbS} = 225$ K; ref. 20), PbSe (diameter = 7.5 nm, $\theta_{D,PbSe} = 175$ K; ref. 20), PbTe (diameter = 7.5 nm, $\theta_{D,PbTe} = 136$ K; ref. 20) and Fe_3O_4 (diameter = 8.0 nm, $\theta_{D,Fe3O4} > 350$ K; ref. 21) NCAs, and Pb oleate ligands. The points have been slightly offset in temperature so error bars can be resolved. T^2 and T^3 scalings are included for reference. **d**, Normalized temperature series for Pb oleate ligands and PbSe and Fe_3O_4 NCAs (with the respect to their maximum thermal conductivity) plateau above 150 K for Pb oleate, 200 K for PbSe and 300 K for Fe_3O_4 NCA. Error bars represent the uncertainty in FDTR measurements (ref. 12).

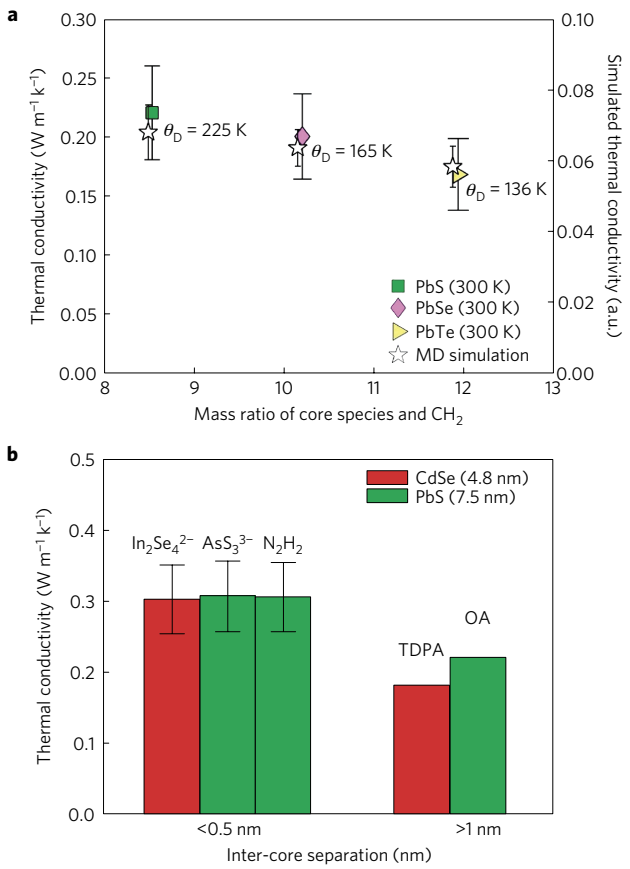

Figure 4 | Effects of NCA chemistry on thermal conductivity. **a**, Oleate-capped lead chalcogenide NCAs show a decrease in thermal conductivity with larger mass ratio, that is, smaller core Debye temperature θ_D (θ_D from ref. 20). The molecular dynamics (MD) simulation data are displaced horizontally for clarity. **b**, NCA thermal conductivity for different inorganic ($In_2Se_4^{2-}$, AsS_3^{3-}, N_2H_4) and organic ligands (tetradecylphosphonic acid (TDPA) and oleic acid (OA)) on CdSe and PbS nanocrystals. Shorter inorganic ligands increase the thermal conductivity by 50% relative to organic ligands. Error bars represent the uncertainty in FDTR measurements (ref. 12).

Supplementary Information). The dominance of elastic scattering events at the interfaces in the NCA is supported by experimental Au/alkanedithiol/GaAs SAM junction thermal conductances, which plateau above a temperature of 200 K (ref. 22). If inelastic events were present at the interface, then the thermal conductance would continue to increase with increasing temperature[23]. We also observe that the thermal conductivity scales as T^{α} below a temperature of 50 K, where $2 < \alpha < 3$, a scaling that requires further investigation.

Core–ligand chemistry defines the electronic properties of NCAs (ref. 2). For example, the electronic conductivity of a PbSe NCA recorded a ten order of magnitude increase by exchanging the oleic acid ligands with shorter hydrazine molecules[1,2]. To determine whether thermal transport parallels charge transport, core and ligand chemistries were systematically changed. Lead chalcogenide (PbS, PbSe and PbTe cores, all 7.5 nm in diameter) NCAs were chosen to isolate the effect of core species as they can be prepared with the same oleate ligand group. The experimental thermal conductivity results are plotted in Fig. 4a versus the mass ratio of the core species (species average) and the methylene group (CH_2) of the ligand. A decreasing thermal conductivity with increasing mass ratio is observed. This result corresponds to a decreasing thermal conductivity with decreasing θ_D (that is, heavier core species). The 30% reduction for PbS versus PbTe NCAs cannot be solely explained by the reduced bulk thermal conductivity of PbS versus PbTe, which amounts to only a 5% change in k_{NCA} (based on HJ–ME; ref. 24). Furthermore, lower θ_D identifies a shift of core phonons to lower-frequency states having less overlap with the high-frequency ligand states. Theory suggests that this misalignment will reduce h (ref. 25) and on the basis of k_{NCA} data, HJ–ME indicates that h is reduced from 140^{+170}_{-80} MW m^{-2} K^{-1} for PbS to 72^{+57}_{-34} MW m^{-2} K^{-1} for PbTe NCAs.

The role of ligand chemistry in NCA thermal transport was elucidated by exchanging the long organic ligands with short inorganic ligands (N_2H_4, AsS_3^{3-}, $In_2Se_4^{2-}$) on PbS and CdSe nanocrystals originally capped with oleate and *n*-tetradecylphosphonate ligands, respectively. The thermal conductivities increased by 50% after the ligand exchange, as shown in Fig. 4b. NCAs with long organic ligands are electrically insulating, inhibiting electrons as potential heat carriers. NCAs with short inorganic ligands, however, have such a small inter-core separation that electronic coupling between neighbouring nanocrystals has been reported[6]. Using the Wiedemann–Franz law for PbSe–N_2H_4 and CdSe–$In_2Se_4^{2-}$ NCAs (refs 5,6), we estimate electronic thermal conductivities of 6.2×10^{-3} W m^{-1} K^{-1} and 2.7×10^{-2} W m^{-1} K^{-1} based on their electrical conductivities. These estimates are at least an order of magnitude smaller than our measured values, verifying that electronic contributions to k_{NCA} are negligible.

Despite higher interface density and absent electronic contributions, several explanations for increased k_{NCA} in Fig. 4b may be at play within the framework of HJ–ME. Using PbS nanocrystals capped with N_2H_4 or oleate ligands as an example, the shorter N_2H_4 ligands have a higher bulk thermal conductivity[26] than oleic acid[13]. Contraction of the NCA structure due to shorter ligands increases the core volume fraction for PbS (7.5 nm) from 0.43 to 0.61, which alone results in an increased HJ–ME prediction from 0.22 to 0.28 W m^{-1} K^{-1}. Finally, the value of h may increase owing to improved alignment of the core–ligand vibrational states resulting from heavier ligand atoms.

To gain further insight into the thermal conductivity measurements, molecular dynamics simulations were performed on a simplified non-dimensionalized NCA model as shown in Supplementary Fig. S5 (see Supplementary Information for details). This model mirrors several salient features of real NCAs. Notably, a similar mass ratio of the core and ligand species, overlapping ligands between neighbouring nanocrystals, and weak inter-ligand interactions. In Figs 3a, 4a and Supplementary Fig. S3a, the simulation results are plotted alongside the measurements. Although the simulation values cannot be directly compared with experiments, the non-dimensionalized predictions show similar trends in film thickness, nanocrystal diameter and mass ratio. Perhaps the most enlightening result is the temperature profile in Supplementary Fig. S5, where all of the temperature drops occur across the ligand junctions between the isothermal cores. This behaviour supports our experimental conclusion that thermal transport is ligand mediated, and on the basis of the mass ratio results, influenced by h.

We have shown that the NCA thermal conductivity is mitigated by the overlap and coupling of the core and ligand vibrational states and the volume fractions of the constituents. On the basis of our measurements, the temperature gradient within a NCA-based light-emitting diode active region or field-effect transistor will be 100–1,000 times higher than in commercial devices that use Si or other single-crystal semiconductors, posing further requirements for thermal management and electronics packaging. Nevertheless, exchanging the long organic ligands with shorter inorganic ligands increases the electrical conductivity by many orders of magnitude[5] with an accompanied increase of only 50% in thermal conductivity. This decoupling of the thermal and electronic properties evokes hope for solution-processable NCA-based thermoelectrics.

Methods

Nanocrystal synthesis. We synthesized highly monodisperse PbS, PbSe, PbTe, CdSe, Au and Fe_3O_4 nanocrystals according to literature methods. Details are given in the Supplementary Information. Briefly, PbS, PbSe and PbTe nanocrystals were synthesized by reacting lead oleate with bis(trimethylsilyl)sulphide, tri-*n*-butylphosphine selenide or tri-*n*-octylphosphine telluride, respectively. CdSe nanocrystals were synthesized from dimethylcadmium and tri-*n*-octylphosphine selenide at 300 °C in the presence of *n*-alkylphosphonic acid, trioctylphosphine and hexadecylamine. Fe_3O_4 nanocrystals were synthesized by controlled thermal decomposition of iron oleate in 1-octadecene.

Ligand exchanges. Na_3AsS_3-capped PbS nanocrystals were prepared according to the method in ref. 27, and redispersed in dimethylformamide. The $(N_2H_5)_2In_2Se_4$-capped CdSe nanocrystals were prepared according to the method in ref. 28. A solid-state ligand exchange with N_2H_4 was carried out on PbS NCAs to partially remove the oleic acid ligands according to the method in ref. 1. Further details are provided in the Supplementary Information.

NCA preparation. NCAs were prepared by spin-casting (18 s at 1,000 r.p.m. followed by 60 s at 1,500 r.p.m.) concentrated (15–60 mg ml^{-1}) colloidal solutions in chloroform or chlorobenzene for organic-capped nanoparticles, dimethylformamide for Na_3AsS_3-capped PbS nanocrystals and hydrazine for $(N_2H_5)_2In_2Se_4$-capped CdSe nanocrystals on polished Si wafers. For the organic-capped samples the native oxide on the Si was etched by treating with 4% HF solution for 2–3 min before rinsing with deionized water and drying under N_2 flow. For the inorganically capped nanocrystals, the Si wafers were oxygen plasma treated for 5 min. A layer of Au was deposited on the PbS, PbSe, PbTe, CdSe and Fe_3O_4 samples using an electron-beam evaporator whereas a thermal evaporator was used for the Au samples where the substrate was cooled with liquid N_2.

Characterization. The size of the nanocrystal cores was determined using the relations between the absorption maximum and nanocrystal size for lead- and cadmium chalcogenide nanocrystals and/or transmission electron microscopy (TEM). Absorption spectra were collected on a ultraviolet–visible–near-infrared spectrophotometer (Cary 5000). TEM images were collected on an FEI Tecnai F30 microscope. Thermal analysis of the NCAs was carried out using both TGA on either a Mettler Toledo 851 or a TA instruments SDT Q600 and DSC on a Mettler Toledo 823.

The NCAs were characterized using scanning electron microscopy (SEM) on a FEI Nova NanoSEM 200 and atomic force microscopy (AFM) on a Nanoscope V (Digital Instruments). The thickness of the films was measured over multiple areas by cleaving the samples in half and imaging at a 90° angle. The surface morphology and root-mean-square roughness was acquired in AFM tapping mode. Further details are provided in the Supplementary Information.

FDTR method. Our FDTR technique, illustrated in Supplementary Fig. S4a, employs two continuous wave lasers (Coherent) to heat the sample and measure its thermal response to identify the unknown NCA thermal conductivity[29]. The 488 nm laser (the pump) is intensity-modulated and periodically heats the gold surface while the 532 nm laser (the probe) continuously monitors the resultant thermal response through the thermoreflectance of the gold layer. The pump is modulated sinusoidally from 100 kHz to 20 MHz. The resulting probe signal is measured using a radiofrequency lock-in amplifier (Stanford Instrument, SR844), producing a set of frequency-dependent phase data, related to the thermal properties of the sample. These data are fitted using a thermal conduction model (see Supplementary Table S1 for fitting parameters) to determine the unknown thermal conductivity of the NCA (ref. 29).

The phase data and fits shown in Supplementary Fig. S4b for a bare silicon substrate and a silicon substrate with a 50 nm PbS NCA film demonstrate the high sensitivity of the FDTR technique to the presence of the NCA film. The resulting thermal conductivity has an uncertainty of 15–20% due to goodness of fit of the model and input parameter uncertainties (NCA film thickness, NCA heat capacity, Si substrate thermal conductivity, Au film thermal conductivity, Au film thickness, laser spot diameter)[12]. To minimize this uncertainty, we separately measured the thermal conductivities of the Si substrate (using FDTR) and gold film (using either FDTR or the Wiedemann–Franz law through sheet resistance measurements made on a dielectric sample that was coated with Au at the same time as the NCAs). The largest uncertainty results from thickness variations in the NCA film, which were quantified to be approximately 10% of the film thickness by both SEM and AFM (see Supplementary Table S2 for sample images).

Experimentally measured heat capacity values were used as input to the heat conduction model for temperatures greater than 150 K. The fitting model is insensitive to the exact NCA heat capacity values at lower temperature. At these low temperatures, changing the heat capacity values by an order of magnitude causes the resultant thermal conductivity value to vary within the experimental error. This is a result of the pump being typically modulated with a period much longer than the NCA film thermal time constant ($\tau = L^2/\alpha$, where L is the NCA film thickness and α is the NCA thermal diffusivity). In this regime the NCA heat capacity becomes unimportant for determining the thermal conductivity because the temperature profile in the film is quasi steady-state. For example, the thermal time constant at temperatures of 150 and 300 K for a 50-nm-thick 7.5-nm-diameter PbS NCA is approximately 19 and 27 ns, restricting the heating frequency to below 52 and 36 MHz for quasi steady behaviour and insensitivity to the NCA heat capacity.

Received 2 July 2012; accepted 5 February 2013; published online 17 March 2013

References

1. Talapin, D. V. & Murray, C. B. PbSe nanocrystal solids for n- and p-channel thin film field-effect transistors. *Science* **310,** 86–89 (2005).
2. Talapin, D. V., Lee, J-S., Kovalenko, M. V. & Shevchenko, E. V. Prospects of colloidal nanocrystals for electronic and optoelectronic applications. *Chem. Rev.* **110,** 389–458 (2010).
3. Gur, I., Fromer, N. A., Geier, M. L. & Alivisatos, A. P. Air-stable all-inorganic nanocrystal solar cells processed from solution. *Science* **310,** 462–465 (2005).
4. Briseno, A. L. & Yang, P. Optoelectronics: Combining chemical worlds. *Nature Mater.* **8,** 7–8 (2009).
5. Coe, S., Woo, W-K., Bawendi, M. & Bulović, V. Electroluminescence from single monolayers of nanocrystals in molecular organic devices. *Nature* **420,** 800–803 (2002).
6. Lee, J-S., Kovalenko, M. V., Huang, J., Chung, D. S. & Talapin, D. V. Band-like transport, high electron mobility and high photoconductivity in all-inorganic nanocrystal arrays. *Nature Nanotech.* **6,** 348–352 (2011).
7. Murray, C. B., Kagan, C. R. & Bawendi, M. G. Self-organization of CdSe nanocrystallites into three-dimensional quantum dot superlattices. *Science* **270,** 1335–1338 (1995).
8. Burda, C., Chen, X., Narayanan, R. & El-Sayed, M. A. Chemistry and properties of nanocrystals of different shapes. *Chem. Rev.* **105,** 1025–1102 (2005).
9. Losego, M. D., Grady, M. E., Sottos, N. R., Cahill, D. G. & Braun, P. V. Effects of chemical bonding on heat transport across interfaces. *Nature Mater.* **11,** 502–506 (2012).
10. Höhne, G. W. H., Hemminger, W. F. & Flammersheim, H-J. *Differential Scanning Calorimetry* 2nd edn (Springer, 2003).
11. Terrill, R. H. *et al.* Monolayers in three dimensions: NMR, SAXS, thermal, and electron hopping studies of alkanethiol stabilized gold clusters. *J. Am. Chem. Soc.* **117,** 12537–12548 (1995).
12. Malen, J. A. *et al.* Optical measurement of thermal conductivity using fiber aligned frequency domain thermoreflectance. *J. Heat Transfer* **133,** 081601 (2011).
13. Baroncini, C., Filippo, P., Latini, G. & Pacetti, M. Organic liquid thermal conductivity: A prediction method in the reduced temperature range 0.3 to 0.8. *Int. J. Thermophys.* **2,** 21–38 (1981).
14. Wang, J., Carson, J. K., North, M. F. & Cleland, D. J. A new approach to modelling the effective thermal conductivity of heterogeneous materials. *Int. J. Heat Mass Transfer* **49,** 3075–3083 (2006).
15. Hasselman, D. P. H. & Johnson, L. F. Effective thermal conductivity of composites with interfacial thermal barrier resistance. *J. Compos. Mater.* **21,** 508–515 (1987).
16. Wang, Z. *et al.* Ultrafast flash thermal conductance of molecular chains. *Science* **317,** 787–790 (2007).
17. Wang, R. Y., Segalman, R. A. & Majumdar, A. Room temperature thermal conductance of alkanedithiol self-assembled monolayers. *Appl. Phys. Lett.* **89,** 173113 (2006).
18. Minnich, A. & Chen, G. Modified effective medium formulation for the thermal conductivity of nanocomposites. *Appl. Phys. Lett.* **91,** 073105 (2007).
19. Cline, C. F., Dunegan, H. L. & Henderson, G. W. Elastic constants of hexagonal BeO, ZnS, and CdSe. *J. Appl. Phys.* **38,** 1944–1948 (1967).
20. Parkinson, D. H. & Quarrington, J. E. The molar heats of lead sulphide, selenide and telluride in the temperature range 20 K to 260 K. *Proc. Phys. Soc. A* **67,** 569–579 (1954).
21. Kouvel, J. Specific heat of a magnetite crystal at liquid helium temperatures. *Phys. Rev.* **102,** 1489–1490 (1956).
22. Luo, T. & Lloyd, J. R. Equilibrium molecular dynamics study of lattice thermal conductivity/conductance of Au–SAM–Au junctions. *J. Heat Transfer* **132,** 032401 (2010).
23. Hopkins, P. E., Norris, P. M. & Stevens, R. J. Influence of inelastic scattering at metal-dielectric interfaces. *J. Heat Transfer* **130,** 022401 (2008).
24. Pei, Y-L. & Liu, Y. Electrical and thermal transport properties of Pb-based chalcogenides: PbTe, PbSe, and PbS. *J. Alloys Comp.* **514,** 40–44 (2012).
25. Segal, D. & Nitzan, A. Heat rectification in molecular junctions. *J. Chem. Phys.* **122,** 194704 (2005).
26. Safarov, M. M. & Zaripova, M. A. Density dependence of heat conductivity of aqueous hydrazine solutions within wide ranges of temperature and pressure. *J. Eng. Phys. Thermophys.* **68,** 390–394 (1996).

27. Kovalenko, M. V., Bodnarchuk, M. I., Zaumseil, J., Lee, J-S. & Talapin, D. V. Expanding the chemical versatility of colloidal nanocrystals capped with molecular metal chalcogenide ligands. *J. Am. Chem. Soc.* **132,** 10085–10092 (2010).
28. Kovalenko, M. V., Scheele, M. & Talapin, D. V. Colloidal nanocrystals with molecular metal chalcogenide surface ligands. *Science* **324,** 1417–1420 (2009).
29. Cahill, D. G. Analysis of heat flow in layered structures for time-domain thermoreflectance. *Rev. Sci. Instrum.* **75,** 5119–5112 (2004).
30. Harikrishnan, S. & Kalaiselvam, S. Preparation and thermal characteristics of CuO–oleic acid nanofluids as a phase change material. *Thermochim. Acta* **533,** 46–55 (2012).
31. Hashin, Z. Assessment of the self consistent scheme approximation: Conductivity of particulate composites. *J. Compos. Mater.* **2,** 284–300 (1968).

Acknowledgements

We thank M. V. Kovalenko, A. Ruditskiy and J. M. Kurley for the synthesis of CdSe nanocrystals, and S. Wyant and S. Majumdar for help in FDTR preparations. S.M.R. and D.V.T. acknowledge support from the II-VI Foundation and NSF CAREER Award (DMR-0847535). J.A.M. and W-L.O. acknowledge support from the AFOSR Young Investigator Program (FA95501110030) and the NSF CAREER Award (ENG-1149374). A.J.H.M. acknowledges support from the AFOSR Young Investigator Program (FA95501010098). This work used facilities supported by the NSF MRSEC Program under Award Number DMR-0213745 and the facilities at the Center for Nanoscale Materials, a US Department of Energy, Office of Science, Office of Basic Energy Sciences User Facility under Contract No. DE-AC02-06CH11357.

Author contributions

W-L.O. conducted the FDTR measurements on the NCAs, molecular dynamics simulations and lattice dynamics calculations. S.M.R. synthesized NCAs, conducted TGA, DSC and absorption spectra measurements, and took SEM, TEM and AFM images. W-L.O. and S.M.R. wrote the paper. D.V.T., A.J.H.M. and J.A.M. edited the paper. All authors discussed the data and commented on the manuscript.

Additional information

Supplementary information is available in the online version of the paper. Reprints and permissions information is available online at www.nature.com/reprints. Correspondence and requests for materials should be addressed to D.V.T. or J.A.M.

Competing financial interests

The authors declare no competing financial interests.